OPEN ACCESS
Fractals, Vol. 31, No. 8 (2023) 2340173 (17 pages)

DOI: 10.1142/S0218348X23401734

A NEW SEVEN-REGION FLOW MODEL FOR DELIVERABILITY EVALUATION OF MULTIPLY-FRACTURED HORIZONTAL WELLS IN TIGHT OIL FRACTAL RESERVOIR

FANRONG GUO,* ROU CHEN,* WEIWEI YAN,*,†,§,‖
YING SU,‡ YANYAN HU‡ and SHENGCHUN XIONG‡,¶,‖
*College of Metrology and Measurement Engineering
China Jiliang University, Hangzhou 310018, P. R. China
†School of Mechanical and Aerospace Engineering
Nanyang Technological University, Singapore 639798, Singapore
‡Research Institute of Petroleum Exploration and Development
PetroChina, Beijing 100089, P. R. China
§yanww@cjlu.edu.cn
¶xiongshengchun@petrochina.com.cn

Received November 29, 2022
Accepted February 15, 2023
Published August 18, 2023

Abstract

Deliverability evaluation plays an important role in the reservoir exploitation. In this study, a new seven-region semi-analytical mathematical model considering the influences of fractal, imbibition and non-Darcy flow is proposed to evaluate the deliverability of multiply-fractured horizontal wells in tight oil reservoirs. The Laplace transformation, perturbation method and Stehfest numerical inversion are employed to solve the model. The reliability and accuracy of

‖Corresponding authors.

the analytical solution are verified by the field example. The sensitivity analysis of the major influencing factors on the deliverability is specifically analyzed. The numerical results indicate that the seven-region semi-analytical model can better explain the heterogeneity of fracture network, and its solution can provide an effective algorithm for the deliverability evaluation. It is found that the fractal plays a predominant influence on the productivity of tight oil reservoirs. The larger the fractal dimension and the smaller the fractal index, the higher the accumulative production rate. The imbibition also has an important effect on the deliverability of tight oil reservoirs. As the rising of wetting angle, both daily and accumulative production rates can obviously decrease. The imbibition has a positive impact on the production rate in the water-wet formations, while it has a negative impact on the production rate in the oil-wet formations. Compared with the fractal and imbibition, the threshold pressure gradient has less influence on the production of tight oil reservoirs. There exists a negative correlation between the threshold pressure gradient and the production performance. This work provides a new approach to understand the fractal tight oil reservoirs, which is of great significance for the deliverability evaluation.

Keywords: Tight Oil Reservoir; Deliverability Evaluation; Fractal; Imbibition; Non-Darcy Flow.

1. INTRODUCTION

The technology of multiply-fractured horizontal wells (MFHW) is widely used in petroleum research due to its economic viability and high efficiency for the unconventional resources. In general, multi-staged hydraulic fracturing not only produces fractures with high conductivity, but also communicates with natural fractures, resulting in complex secondary fractures and fracture network which greatly improves the reservoir permeability.[1–4] The tight oil reservoir with complex and heterogeneous fracture network is formed by the hydraulic-induced fractures and the activated natural fractures around the horizontal wells. However, many mechanisms of the fluid flow are still not clear, such as the relationship of the complex flow interplay among matrix, natural fractures, hydraulic fractures and horizontal wellbores, which makes the production behavior and pressure-transient flow by analytical models much more complicated.[5]

Numerical models are widely applied in the flow simulation of volume-fractured horizontal wells, of which the analytical/semi-analytical models are mainly linear flow models.[6–8] Even though the numerical models were developed to analyze the unconventional reservoirs, it can be constrained by computer calculation ability and the uncertainty evaluation process is time-consuming. Thus, various analytical oil flow models of MFHW were developed based on the classical trilinear-flow model,[9] in which the fluid flow process can be divided into three different continuous regions: the outer reservoir, the inner reservoir between hydraulic fractures, and the hydraulic fracture zone with finite conductivity. After that, an enhanced fractured trilinear-flow model assuming all the fractures with the same length and conductivity was proposed, whose difference from the classical model was the reservoir structure.[10] Recently, a five-region multi-linear seepage model of fractured horizontal well in a closed homogeneous layer is established,[11] which subdivides the reservoir into five regions and can be used for more complex homogeneous reservoirs.

An optimized work of five-linear-region semi-analytical model for production performance analysis of MFHW in tight oil reservoirs was proposed by Ji *et al.*,[12] where the influence of non-Darcy flow in the unstimulated reservoir volume (USRV) and the stress sensitivity without imbibition were considered. The stimulated reservoir volume (SRV) in this model was an idealized dual-porous medium area, which was subdivided into two areas (SRV and partial SRV) and good forecasting reservoirs productivity was obtained. Yuan *et al.*[13] established a seven-region multi-linear flow model to study the interplay between flowing pressure and production rate for horizontal wells in tight gas reservoirs, which was proved to be more realistic and possess practical application than the trilinear-flow model after considering the effects of fracture intensity, threshold pressure gradient, compaction and size of SRV on accumulative productivity. Though the flow models mentioned above were sufficient to describe some key features of flow convergence towards the

fractured horizontal wells, they could not consider the heterogeneity of the SRV region and non-continuum flows because they cannot provide sufficient details of complex fracture network structure and fluid flow characteristics in tight oil reservoirs.

Fractal geometry is found to be a better method to describe those discontinuous, abrupt and rough complex objects.[14,15] To date, fractal theory has been successfully applied to productivity evaluation and pressure analysis of oil and gas reservoirs, which presents a good method to further describe the heterogeneity of actual complex fracture networks. Katz and Thompson[16] used optical data to demonstrate the pore spaces of sandstone were fractal geometries and were high self-similarity in length. Chang and Yortsos[17] analyzed pressure-transient response in a fractal reservoir under the condition of matrix participation or both the fracture network and matrix, which gave a unified description for the single and dual-porosity system. Their result could be used to identify and model naturally fractured reservoirs with multiple property scales. After that, a synthetic network of fractures with fractal characteristics was numerically constructed, which suggested that there existed a power law in the mass–radius relationship around the test well location.[18] Cossio *et al.*[19] first applied the fractal theory to obtain semi-analytical fractal-fracture solution for the classic trilinear model in a homogeneous infinite-acting reservoir. In addition, some researchers established analytical models for vertically fractured wells with dual-porosity models to simulate the flow in the SRV.[20] Though these studies were focused on the complex network with heterogeneity, all of them ignored imbibition effect on fractured reservoir exploitation performances and needed to be further improved.[21–26]

In this work, the fractal permeability and fractal porosity are introduced to characterize the heterogeneity of fracture parameters in the USR, and the influence of non-Darcy flow is considered in the USRV for its ultra-low permeability. Furthermore, the imbibition effect on the fractured reservoir exploitation performances is also taken into account. We propose a new seven-region semi-analytical mathematical model in a fractal oil reservoir to explore the influence law of the heterogeneous fracture parameters on the productivity of MFHW. This work will provide a novel way to understand the fractal tight oil reservoirs, which is of great significance for the deliverability evaluation.

2. MODEL CONSTRUCTION

2.1. Physical Model and Assumptions

Large-scale hydraulic fracturing can create secondary fractures along with primary fractures in tight oil reservoir and forms complex fracture networks. To characterize the heterogeneity of fractured reservoir and the complexity of fracture network, the fractal permeability and fractal porosity are introduced. A productivity model for the MFHW based on the fractal, imbibition and threshold pressure gradient is established to explore the effects of fractal, imbibition and non-Darcy flow on the productivity of horizontal well. The reservoir is subdivided into seven continuous regions, as illustrated in Fig. 1. (1) Fracture region (Region 1): Fluid permeability is high and no threshold pressure gradient is considered; one-dimensional fluid linear flow along with fracture orientation is assumed, and the skin and wellbore storage effects are considered. (2) Deformable double media imbibition region (Region 2): In the existing fractures and matrix, the fracturing fluid sweeps into the region and there exist both imbibition and cross-flow in this zone. Assuming one-dimensional fluid linear flow, the fractal dimension and capillary pressure are incorporated. (3) Double fracture network area (Region 3): It is the secondary fracture area of the SRV. We assume one-dimensional linear flow in the x-direction, and consider non-Darcy flow, fractal dimension and anomalous diffusion coefficient to describe the seepage characteristics in the complex fracture network. (4) Regions 4–7 are the USRV with low permeability, where threshold pressure gradient exists to describe the non-Darcy flow in the areas.

The following basic techniques are applied to describe the complex tight oil reservoir.

Fractal theory: Fractal theory is used to describe the porosity and permeability of complex fracture network. Strong heterogeneity of fracture is exhibited in various natural fractures caused by the impact of reservoir rock mechanical parameters.

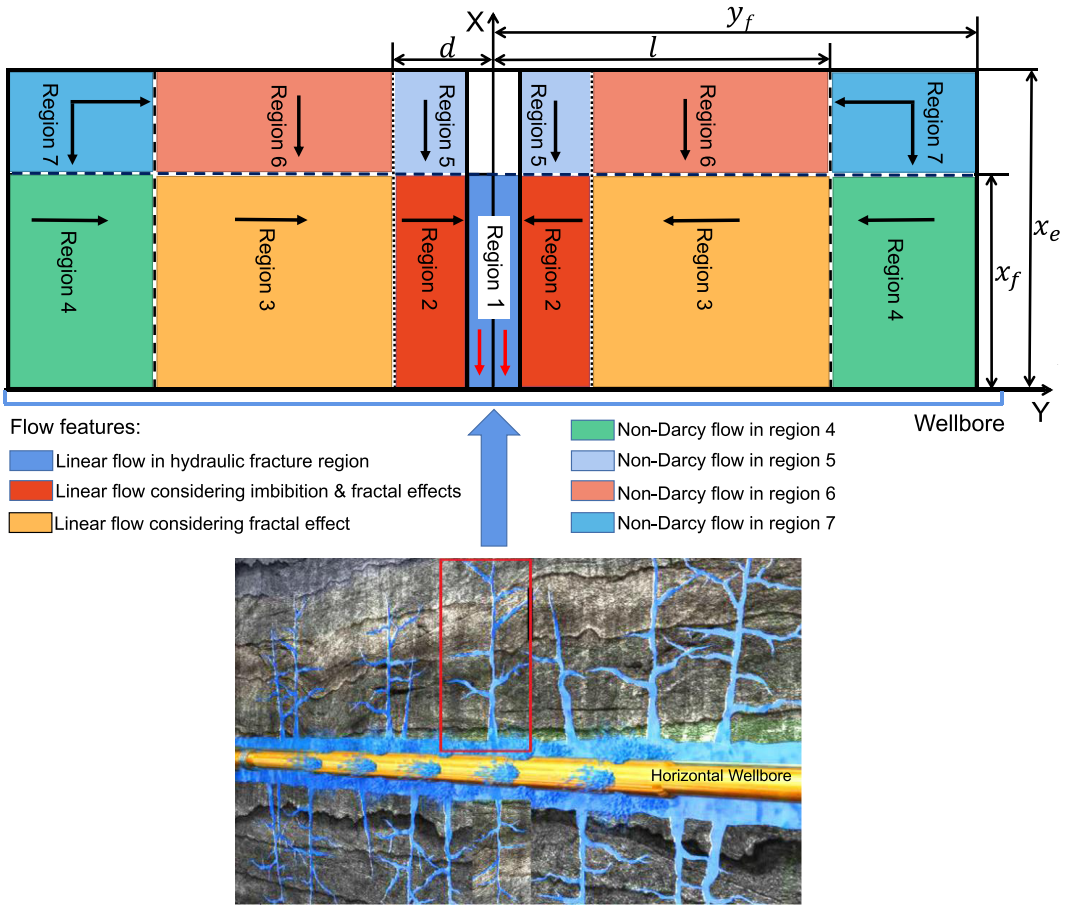

Fig. 1 Physical model of MFHW in tight oil fractal reservoirs.

Therefore, it is impossible for fractures to completely communicate with artificial fractures in the reservoir stimulated area. The power-law functions are applied for the fractal permeability and porosity to derive the fractal fracture diffusivity equation. As for the fracture system, the permeability k_f and porosity ϕ_f are given as[27]

$$\begin{aligned} k_f &= k_{fw}(y/y_w)^{D_f-2-\theta_f}, \\ \phi_f &= \phi_{fw}(y/y_w)^{D_f-2}, \end{aligned} \tag{1}$$

where y_w is a side length of a region where fracture porosity is ϕ_{fw} and permeability k_{fw}; D_f and θ_f are the fractal dimension and fractal index in the fracture system, respectively. Similarly, for the matrix system, the fractal permeability k_m and porosity ϕ_m are defined as

$$\begin{aligned} k_m &= k_{mw}(y/y_w)^{D_m-2-\theta_m}, \\ \phi_m &= \phi_{mw}(y/y_w)^{D_m-2}, \end{aligned} \tag{2}$$

where D_m and θ_m are the fractal dimension and fractal index in the matrix system. These four parameters characterize the porosity and permeability fractal properties of the matrix and fracture system.

Capillary pressure: From the microscopic point of view, the fluid flow in the reservoir is the fluid flow in single-phase and multi-phase capillary bundles. Thus, not only Darcy's theorem but also the capillary pressure should be considered. The capillary pressure is high in the matrix in tight oil reservoir with high heterogeneity, while in fractures or wellbore it is negligible. In this work, the capillary pressure term is added into the inter-porosity term of dual-porosity reservoir to characterize imbibition effect. For tortuous capillaries with variably shaped apertures, the capillary pressure p_c is a function of saturation S_{wD}, wettability angle β and interfacial tension σ, which can be expressed by

$$p_c = AS_{wD}^{B}\sigma\cos\beta\sqrt{\frac{\phi}{k}}, \tag{3}$$

where both A and B are the regression coefficients.[28,29]

Non-Darcy flow: To consider the non-Darcy flow in the USRV, the Pseudo-TPG method is used, which is defined by[12,30]

$$v = \begin{cases} -\dfrac{3.6k}{\mu}(\nabla p - G), & \nabla p > G, \\ 0, & \nabla p \le G, \end{cases} \tag{4}$$

where G is the Pseudo-TPG. Fluid flow in the model is treated as a combination of seven flows within contiguous regions.

Due to the symmetry of the system, we just need to build the diffusion equations on one-quarter of the space between the fractures, and solutions for each region can be obtained by imposing flux and pressure continuity across the boundaries between different adjacent regions. To derive the analytical model conveniently, the basic assumptions about this physical model are presented as follows: (1) The tight oil reservoir is a homogeneous box-shaped formation, where the upper and lower boundaries are closed, which means no flow velocity in the middle of adjacent fractures. (2) The MFHW is located in the center of the oil reservoir, and the initial pressure is kept equal in different regions. (3) Hydraulically primary fractures are treated as symmetrical wing fractures perpendicular to the horizontal wellbore and the fractures penetrate the formation entirely. All hydraulic fractures have the same length and conductivity and are spaced uniformly along the horizontal well. (4) The fluid could only flow towards the wellbore through primary fractures. The effect of gravity and pressure loss along the horizontal wellbore is neglected. (5) Capillary pressure is considered in Region 2 due to the imbibition. The effect of imbibition is mainly reflected by wettability. To obtain an analytical solution of the mathematical model, it is worth mentioning that the fluid in each rock pore is assumed to flow into the fracture, and the fractal dimension of the fractured medium D_f is equal to that of the matrix D_m. These assumptions are practical because they ensure the fluid in each matrix pore can seep into the fracture system. For the fractal dual-porosity reservoir model, the fractal permeability and porosity of matrix system are often neglected. One reason is to facilitate mathematical modeling, another reason is that the matrix permeability is very small compared with the fracture, and the fluid mainly flows through the fracture, so the fractal effect is mainly reflected in the fracture system. The fractal index of the matrix θ_m is equal to 0, which means there is no abnormal conductivity in the rock medium fractals.

Table 1 Definitions of Dimensionless Variables. Here, i Represents Different Regions with $i = 1-7$.

Variable	Definition	Variable	Definition
p_{iD}	$\frac{k_{2f}h(p_0-p_i)}{q\mu B}$	t_D	$\frac{3.6k_{2f}t}{(\phi C_t)_2\mu x_f^2}$
x_D	$\frac{x}{x_f}$	y_D	$\frac{y}{x_f}$
w_D	$\frac{w_f}{x_f}$	l_D	$\frac{l}{x_f}$
G_{iD}	$C_{l2f}x_fG_i$	g_{iD}	$-\frac{k_{2f}hx_fG_i}{q\mu B}$
p_{cD}	$-\frac{k_{2f}h(p_0-p_i)}{q\mu B}p_c$	q_D	$\frac{\mu B}{k_{2f}h(p_0-p_{wf})}q$

2.2. Mathematical Model in Each Region

Before obtaining fluid governing equations in different regions, we introduce dimensionless variables, which are used to simplify the calculation of mathematical models. The dimensionless parameters are defined in Table 1.

(1) Region 1: Region 1 is the primary hydraulic fracture area, where the flow is assumed to be linear flow in the x-direction. The diffusion equation is obtained by

$$\frac{k_{10}}{\mu_1}\frac{\partial^2 p_1}{\partial x^2} + q_{12} = \frac{\phi_1 C_{t1}}{3.6}\frac{\partial p_1}{\partial t}, \tag{5}$$

where q_{12} is the supplement flow term from Region 2 to Region 1. The inner reservoir boundary is $\frac{\partial p_1}{\partial x}|_{x=0} = \frac{q\mu_1 B}{2k_1 w_f h}$, and the outer reservoir boundary $\frac{\partial p_1}{\partial x}|_{x=x_f} = 0$. Based on the definitions of dimensionless variables (Table 1) and the boundary conditions, the dimensionless diffusion equation and boundary conditions in Region 1 can be obtained by

$$\begin{cases} \dfrac{\partial^2 p_{1D}}{\partial x_D^2} + \dfrac{2\mu_1 k_{2f0}}{\mu_2 k_1 w_{fD}}\dfrac{\partial p_{2fD}}{\partial y_D}\Big|_{y_D=\frac{w_{fD}}{2}} \\ \qquad = \dfrac{\phi_1\mu_1 C_{t1}k_{2f0}}{(\phi C_t)_2\mu_2 k_1}\dfrac{\partial p_{1D}}{\partial t_D}, \\ \dfrac{\partial p_{1D}}{\partial x_D}\Big|_{x_D=0} = -\dfrac{k_{2f}\mu_1}{2k_1\mu_2 w_{fD}}, \\ \dfrac{\partial p_{1D}}{\partial x_D}\Big|_{x_D=x_{fD}} = 0, \quad p_{1D}|_{t_D=0} = 0. \end{cases} \tag{6}$$

(2) Region 2: Region 2 is the deformable double media imbibition region, where both fractures and matrix exist, and the fracturing fluid sweeps into the region causing both imbibition and cross-flow.

To understand the imbibition effect, the capillary pressure is used to represent imbibition intensity in terms of capillary pressure between the matrix and fracture with the assumption of linear flow in the y-direction. To provide a more precise description of the heterogeneity of tight oil reservoirs, the fractal theory, which is based on the self-similarity and scale invariance of the fracture network, is introduced.

For the matrix system, the governing equation is expressed by

$$\frac{\phi_{2m}C_{t2m}}{3.6}\frac{\partial p_{2m}}{\partial t}+\frac{\alpha k_{2m}}{\mu_2}(p_{2m}-p_{2f}+p_c)=0. \quad (7)$$

For the fracture system, the governing equation is given by

$$\begin{aligned}&\frac{\partial^2 p_{2f}}{\partial y^2}+\frac{D-\theta_f-2}{y}\frac{\partial p_f}{\partial y}+\left(\frac{y}{w_f}\right)^{\theta_f}\frac{1}{x_f}\frac{\mu_2 k_{mw}}{k_{fw}\mu_5}\\&\quad\times\left(\frac{\partial p_5}{\partial x}-G_5\right)\Big|_{x=x_f}+\left(\frac{y}{w_f}\right)^{\theta_f}\alpha\frac{k_{2m}}{k_{2f}}\\&\quad\times(p_{2m}-p_{2f}+p_c)=\left(\frac{y}{w_f}\right)^{\theta_f}\frac{\phi_{2f}C_{t2f}\mu_2}{3.6k_{2f}}\frac{\partial p_{2f}}{\partial t}.\end{aligned} \quad (8)$$

The inner reservoir boundary (pressure continuity) is $p_{2f}|_{y=\frac{w_f}{2}}=p_1|_{y=\frac{w_f}{2}}$, and the outer reservoir boundary (flux continuity) is $\frac{k_{2f}}{\mu_2}\frac{\partial p_{2f}}{\partial y}|_{y=d}=\frac{k_{3f}}{\mu_3}\frac{\partial p_{3f}}{\partial y}|_{y=d}$. Substituting Eq. (7) into Eq. (8) and applying to the definition of dimensionless parameters in Table 1, the dimensionless fractal diffusion equation and boundary conditions in Region 2 become

$$\begin{cases}\dfrac{\partial^2 p_{2fD}}{\partial y_D^2}+\dfrac{D-\theta-2}{y_D}\dfrac{\partial p_{2fD}}{\partial y_D}\\\qquad+\lambda_2\left(\dfrac{y_D}{w_{fD}/2}\right)^{\theta_f}(p_{mD}-p_{fD}+p_{cD})\\\qquad+\left(\dfrac{y_D}{w_{fD}/2}\right)^{\theta_f}\dfrac{k_{mw}}{k_{f_w}}\left(\dfrac{\partial p_5}{\partial x}-G_5\right)\Big|_{x=x_f}\\\quad=\left(\dfrac{y_D}{w_{fD}/2}\right)^{\theta_f}\dfrac{\phi_{2f0}C_{t2f}}{(\phi c_t)_2}\dfrac{\partial p_{2fD}}{\partial t_D},\\p_{2fD}|_{y_D=\frac{w_{fD}}{2}}=p_{1D}|_{y_D=\frac{w_{fD}}{2}},\\\dfrac{k_{2f}}{\mu_2}\dfrac{\partial p_{2fD}}{\partial y_D}\Big|_{y_D=d_D}=\dfrac{k_{3f}}{\mu_3}\dfrac{\partial p_{3fD}}{\partial y_D}\Big|_{y_D=d_D},\\p_{2D}|_{t_D=0}=0.\end{cases} \quad (9)$$

(3) Region 3: The fluid is assumed to be linear flow along the x-direction in the RSV. The fractal dimension D_3 and fractal index θ_{3f} are used to describe the heterogeneity of the fracture system.

For the matrix system, the seepage equation is

$$\phi_{3m}C_{t3m}\frac{\partial p_{3m}}{\partial t}+3.6\frac{\alpha k_{3m}}{\mu_3}(p_{3m}-p_{3f})=0. \quad (10)$$

For the fracture system, the seepage equation is

$$\begin{aligned}&\frac{\partial^2 p_{3f}}{\partial y^2}+\frac{D_3-\theta_3-2}{y}\frac{\partial p_{3f}}{\partial y}+\frac{1}{x_f}\frac{k_6}{k_{3f}}\\&\quad\times\left(\frac{y}{w_f}\right)^{\theta_3}\left(\frac{\partial p_6}{\partial x}-G_6\right)\Big|_{x=x_f}\\&\quad+\alpha\frac{k_{3m}}{k_{3f}}\left(\frac{y}{w_f}\right)^{\theta_3}(p_{3m}-p_{3f})\\&\quad=\frac{\phi_{3f}C_{t3f}\mu_3}{3.6k_{3f}}\left(\frac{y}{w_f}\right)^{\theta_3}\frac{\partial p_{3f}}{\partial t}.\end{aligned} \quad (11)$$

According to the definition of dimensionless parameters, the dimensionless fractal diffusion equations and boundary conditions in Region 3 become

$$\begin{cases}(1-\omega_3)\dfrac{\partial p_{3mD}}{\partial t_D}+\lambda_3(p_{3mD}-p_{3fD})=0,\\\dfrac{\partial^2 p_{3fD}}{\partial y_D^2}+\dfrac{D-\theta_f-2}{y_D}\dfrac{\partial p_{3fD}}{\partial y_D}+\lambda_3 y_D^{\theta_f}(p_{3mD}\\\qquad-p_{3fD})+y_D^{\theta_f}\dfrac{k_6}{k_{3f}}\left(\dfrac{\partial p_{6D}}{\partial x_D}-g_{6D}\right)\Big|_{x=x_f}\\\quad=y_D^{\theta_f}\omega_3\dfrac{\partial p_{3fD}}{\partial t_D},\\p_{2fD}|_{y_D=d_D}=p_{3fD}|_{y_D=d_D},\\\dfrac{k_{3f}}{\mu_3}\dfrac{\partial p_{3fD}}{\partial y_D}\Big|_{y_D=l_D}=\dfrac{k_4}{\mu_4}\left(\dfrac{\partial p_{4D}}{\partial y_D}-g_{4D}\right)\Big|_{y_D=l_D},\\p_{3D}|_{t_D=0}=0\end{cases} \quad (12)$$

(4) Region 4: The fluid flows along the y-direction from Region 4 to Region 3. Taking the non-Darcy flow into consideration, the seepage equation can be expressed as

$$\begin{aligned}&\frac{3.6k_4}{\mu_4}\left(\frac{\partial^2 p_4}{\partial y^2}-G_4C_{l4}\frac{\partial p_4}{\partial y}\right)+q_{47}\\&\quad=\phi_4C_{t4}\frac{\partial p_4}{\partial t}.\end{aligned} \quad (13)$$

The dimensionless diffusion equation and boundary conditions in Region 4 are

$$\begin{cases} \dfrac{\partial^2 p_{4D}}{\partial y_D^2} - \dfrac{C_{l4}}{C_{l2f}} G_{4D} \dfrac{\partial p_{4D}}{\partial y_D} \\ \qquad + \dfrac{\mu_4 k_{71}}{\mu_7 k_4} \left(\dfrac{\partial p_{7D}}{\partial x_D} - g_{71D} \right) \Big|_{x_D = x_{fD}} \\ \qquad = \dfrac{\phi_4 \mu_4 C_{t4} k_{2f}}{3.6 k_4 (\phi \mu_2 C_t)_2} \dfrac{\partial p_{4D}}{\partial t_D}, \\ p_{3fD}|_{y=l} = p_{4D}|_{y_D = l_D}, \quad \dfrac{\partial p_{4D}}{\partial y_D}\Big|_{y_D = y_{eD}} = 0, \\ p_{4D}|_{t_D = 0} = 0. \end{cases} \tag{14}$$

(5) Region 5: It is assumed one-dimensional linear flow from Region 5 to Region 2 in the x-direction. Considering the effect of non-Darcy flow, the dimensionless diffusion equation and boundary conditions in Region 5 are

$$\begin{cases} \dfrac{\partial^2 p_{5D}}{\partial x_D^2} - \dfrac{C_{l5}}{C_{l2f}} G_{5D} \dfrac{\partial p_{5D}}{\partial x_D} = \dfrac{k_{2f} \phi_5 \mu_5 C_{t5}}{k_5 (\phi \mu_2 C_t)_2} \dfrac{\partial p_{5D}}{\partial t_D}, \\ p_{2fD}|_{x_D = x_{fD}} = p_{5D}|_{x_D = x_{fD}}, \quad \dfrac{\partial p_{5D}}{\partial x_D}\Big|_{x_D = x_{eD}} = 0, \\ p_{5D}|_{t_D = 0} = 0. \end{cases} \tag{15}$$

(6) Region 6: Similar derivation process like Region 5, considering the non-Darcy flow effect, the dimensionless diffusion equation and boundary conditions in Region 6 are

$$\begin{cases} \dfrac{\partial^2 p_{6D}}{\partial x_D^2} - G_{6D} \dfrac{C_{l6}}{C_{l2f}} \dfrac{\partial p_{6D}}{\partial x_D} \\ \qquad + \dfrac{\mu_6 k_{72}}{k_6 \mu_7 (l_D - d_D)} \left(\dfrac{\partial p_{7D}}{\partial x_D} - g_{72D} \right) \Big|_{y_D = l_D} \\ \qquad = \dfrac{k_{2f} \phi_6 \mu_6 C_{t6}}{(\phi \mu_2 C_t)_2 k_6} \dfrac{\partial p_{6D}}{\partial t_D}, \\ p_{3fD}|_{x_D = x_{fD}} = p_{6D}|_{x_D = x_{fD}}, \\ \dfrac{\partial p_{6D}}{\partial x_D}\Big|_{x_D = x_{eD}} = 0, \quad p_6|_{t_D = 0} = 0. \end{cases} \tag{16}$$

(7) Region 7: Assuming one-dimensional linear flow in both the x-direction and y-direction, considering the non-Darcy flow effect, the dimensionless diffusion equations and boundary conditions in Region 7 are given by

$$\begin{cases} \dfrac{\partial^2 p_{7D}}{\partial x_D^2} - \dfrac{C_{l7}}{C_{l2f}} G_{71D} \dfrac{\partial p_{7D}}{\partial x_D} \\ \qquad = \dfrac{k_{2f} \phi_7 \mu_7 C_{t7}}{k_{71} (\phi \mu_2 C_t)_2} \dfrac{\partial p_{7D}}{\partial t_D}, \\ p_{4D}|_{x_D = x_{fD}} = p_{7D}|_{x_D = x_{fD}}, \\ \dfrac{\partial p_{7D}}{\partial x_D}\Big|_{x_D = x_{eD}} = 0, \quad p_7|_{t_D = 0} = 0. \end{cases} \tag{17}$$

$$\begin{cases} \dfrac{\partial^2 p_{7D}}{\partial y_D^2} - \dfrac{C_{l7}}{C_{l2f}} G_{72D} \dfrac{\partial p_{7D}}{\partial y_D} \\ \qquad = \dfrac{k_{2f} \phi_7 \mu_7 C_{t7}}{k_{72} (\phi \mu_2 C_t)_2} \dfrac{\partial p_{7D}}{\partial t_D}, \\ p_{6D}|_{y_D = l_D} = p_{7D}|_{y_D = l_D}, \\ \dfrac{\partial p_{7D}}{\partial y_D}\Big|_{y_D = y_{eD}} = 0, \quad p_{7D}|_{t_D = 0} = 0. \end{cases} \tag{18}$$

3. RESULTS AND DISCUSSION

To obtain the analytical solutions, the system of equations for each region is first converted to the Laplace domain. According to the different flow directions, solutions of those USRV regions (including Regions 7, 6, 5 and 4) are solved in order. After that, the governing equation in Regions 3 and 2 are derived, respectively. Finally, the analytical horizontal wellbore pressure in Laplace domain is obtained. Figure 2 shows the workflow of solving the analytical pressure and production solution in the multi-linear flow-dominated reservoir.

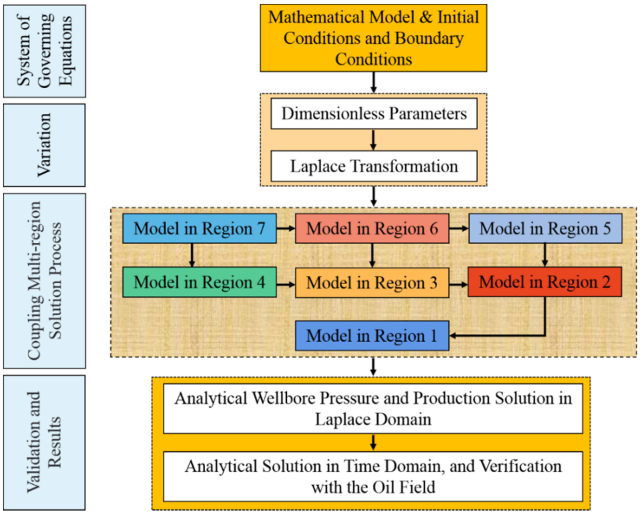

Fig. 2 A workflow to solve for analytical solution in this mathematical model.

3.1. Model Solutions

(1) Solutions of USRV Region

By applying the Laplace transformation to Eq. (17), the dimensionless diffusion equation and boundary conditions in Region 7 in both the x-direction and y-direction are

$$\begin{cases} \dfrac{\partial^2 \bar{p}_{7D}}{\partial x_D^2} - b_{721}\dfrac{\partial \bar{p}_{7D}}{\partial x_D} = \eta_{271} u \bar{p}_{7D}, \\ \bar{p}_{4D}|_{x_D=x_{fD}} = \bar{p}_{7D}|_{x_D=x_{fD}}, \\ \left.\dfrac{\partial \bar{p}_{7D}}{\partial x_D}\right|_{x_D=x_{eD}} = 0, \end{cases} \tag{19}$$

$$\begin{cases} \dfrac{\partial^2 \bar{p}_{7D}}{\partial y_D^2} - b_{722}\dfrac{\partial \bar{p}_{7D}}{\partial y_D} = \eta_{272} u \bar{p}_{7D}, \\ \bar{p}_{6D}|_{y_D=l_D} = \bar{p}_{7D}|_{y_D=l_D}, \\ \left.\dfrac{\partial \bar{p}_{7D}}{\partial y_D}\right|_{y_D=y_{eD}} = 0, \end{cases} \tag{20}$$

where u represents the Laplace variable. The analytical solutions of Eqs. (19) and (20) in Laplace domain can be expressed as follows:

$$\bar{p}_{7D} = \frac{r_{72}\mathrm{e}^{x_D r_{71}} - r_{71}\mathrm{e}^{x_{eD}(r_{71}-r_{72})}\mathrm{e}^{x_D r_{72}}}{r_{72}\mathrm{e}^{r_{71}} - r_{71}\mathrm{e}^{x_{eD}(r_{71}-r_{72})+r_{72}}}\bar{p}_{4D}|_{x_D=x_{fD}}, \tag{21}$$

$$\bar{p}_{7D} = \frac{r_{74}\mathrm{e}^{y_D r_{73}} - r_{73}\mathrm{e}^{y_{eD}(r_{73}-r_{74})}\mathrm{e}^{y_D r_{74}}}{r_{74}\mathrm{e}^{l_D r_{73}} - r_{73}\mathrm{e}^{y_{eD}(r_{73}-r_{74})+l_D r_{74}}}\bar{p}_{6D}|_{y_D=l_D}. \tag{22}$$

Additionally, we have

$$\begin{aligned} \left.\frac{\partial \bar{p}_{7D}}{\partial x_D}\right|_{x_D=x_{fD}} &= F_{74}\bar{p}_{4D}|_{x_D=x_{fD}}, \\ \left.\frac{\partial \bar{p}_{7D}}{\partial y_D}\right|_{y_D=l_D} &= F_{76}\bar{p}_{6D}|_{y_D=l_D}. \end{aligned} \tag{23}$$

As to Region 6, the dimensionless diffusion equation and boundary conditions in the Laplace domain are

$$\begin{cases} \dfrac{\partial^2 \bar{p}_{6D}}{\partial x_D^2} - b_{62}\dfrac{\partial \bar{p}_{6D}}{\partial x_D} - \eta_{26} u \bar{p}_{6D} \\ \qquad + a_{76}\left(\dfrac{\partial \bar{p}_{7D}}{\partial y_D} - \dfrac{g_{72D}}{u}\right)\Big|_{y_D=l_D} = 0, \\ \bar{p}_{3fD}|_{x_D=1} = \bar{p}_{6D}|_{x_D=1}, \quad \left.\dfrac{\partial \bar{p}_{6D}}{\partial x_D}\right|_{x_D=x_{eD}} = 0. \end{cases} \tag{24}$$

Substituting Eqs. (23) into Eqs. (24), the analytical solutions of Region 6 in Laplace domain are given as

$$\begin{cases} \bar{p}_{6D} = \dfrac{[r_{62}\mathrm{e}^{r_{61}x_D} - r_{61}\mathrm{e}^{x_{eD}(r_{61}-r_{62})}\mathrm{e}^{r_{62}x_D}]}{[r_{62}\mathrm{e}^{r_{61}} - r_{61}\mathrm{e}^{x_{eD}(r_{61}-r_{62})}\mathrm{e}^{r_{62}}]} \\ \qquad \times [\bar{p}_{3fD}|_{x_D=x_{fD}} - d_6] + d_6, \\ \left.\dfrac{\partial \bar{p}_{6D}}{\partial x_D}\right|_{x_D=x_{fD}} = F_{63}, \ \ \bar{p}_{3fD}|_{x_D=x_{fD}} - F_{63}d_6. \end{cases} \tag{25}$$

In the same way, the analytical solutions of Region 5 can be given as

$$\begin{cases} \bar{p}_{5D} = \dfrac{[r_{52}\mathrm{e}^{x_D r_{51}} - r_{51}\mathrm{e}^{x_{eD}(r_{51}-r_{52})}\mathrm{e}^{x_D r_{52}}]}{[r_{52}\mathrm{e}^{r_{51}} - r_{51}\mathrm{e}^{x_{eD}(r_{51}-r_{52})}\mathrm{e}^{r_{52}}]} \\ \qquad \times \bar{p}_{2fD}|_{x_D=x_{fD}}, \\ \left.\dfrac{\partial \bar{p}_{5D}}{\partial x_D}\right|_{x_D=x_{fD}} = F_{52}, \ \ \bar{p}_{2fD}|_{x_D=x_{fD}}. \end{cases} \tag{26}$$

Like Region 5, the analytical solutions of Region 4 can be expressed as

$$\begin{cases} \bar{p}_{4D} = \dfrac{r_{42}\mathrm{e}^{y_D r_{41}} - r_{41}\mathrm{e}^{y_{eD}(r_{41}-r_{42})}\mathrm{e}^{y_D r_{42}}}{r_{42}\mathrm{e}^{l_D r_{41}} - r_{41}\mathrm{e}^{y_{eD}(r_{41}-r_{42})}\mathrm{e}^{l_D r_{42}}} \\ \qquad \times (\bar{p}_{3fD}|_{y_D=l_D} - d_4) + d_4, \\ \left.\dfrac{\partial \bar{p}_{4D}}{\partial y_D}\right|_{y_D=l_D} = F_{43}, \ \ \bar{p}_{3fD}|_{y_D=l_D} - F_{43}d_4. \end{cases} \tag{27}$$

(2) Solutions of Region 3

Applying dimensionless variables to Eqs. (12), the dual-porosity fractal model of Region 3 in the Laplace domain can be expressed by

$$\begin{cases} (1-\omega_3)u\bar{p}_{3mD} + \lambda_3(\bar{p}_{3mD} - \bar{p}_{3fD}) = 0 \\ \qquad\qquad\qquad\qquad \text{(matrix system)}, \\ \dfrac{\partial^2 \bar{p}_{3fD}}{\partial y_D^2} + \dfrac{D-\theta_f-2}{y_D}\dfrac{\partial \bar{p}_{3fD}}{\partial y_D} \\ \qquad + y_D^{\theta_f}\, a_{63}\left(\dfrac{\partial \bar{p}_{6D}}{\partial x_D} - \dfrac{g_{6D}}{u}\right)\Big|_{x_D=x_{fD}} \\ \qquad = y_D^{\theta_f} c_3 \bar{p}_{3fD} \quad \text{(fracture system)}, \\ \bar{p}_{2fD}|_{y_D=d_D} = \bar{p}_{3fD}|_{y_D=d_D}, \\ a_{34}\left.\dfrac{\partial \bar{p}_{3fD}}{\partial y_D}\right|_{y_D=l_D} = \left(\dfrac{\partial \bar{p}_{4D}}{\partial y_D} - \dfrac{g_{4D}}{u}\right)\Big|_{y_D=l_D}. \end{cases} \tag{28}$$

Incorporating the seepage equation of matrix system, the governing equation of the fracture system

becomes

$$\frac{\partial^2 \bar{p}_{3fD}}{\partial y_D^2} + \frac{D-\theta_f-2}{y_D}\frac{\partial \bar{p}_{3fD}}{\partial y_D} - w_3\left(\bar{p}_{3fD} + \frac{v_3}{w_3}\right) y_D^{\theta_f} = 0. \quad (29)$$

Based on the general solution of the Bessel function, the general form of solution for Eq. (29) is

$$\overline{p}_{3fD} = y_D^{\frac{3+\theta_3-D_3}{2}}\left[A_3 I_{\frac{3+\theta-D}{2+\theta}}\left(\frac{2w_3^{0.5}}{2+\theta_3} y_D^{\frac{2+\theta_3}{2}}\right) + B_3 K_{\frac{3+\theta-D}{2+\theta}}\left(\frac{2w_3^{0.5}}{2+\theta_3} y_D^{\frac{2+\theta_3}{2}}\right)\right] - \frac{v_3}{w_3}, \quad (30)$$

where $I_{\frac{3+\theta-D}{2+\theta}}(z)$ and $K_{\frac{3+\theta-D}{2+\theta}}(z)$ are the modified Bessel function of the first kind of order $\frac{3+\theta-D}{2+\theta}$. The coefficients A_3 and B_3 can be derived by the boundary conditions. According to Eq. (30), we have

$$\frac{\partial \overline{p}_{3f}}{\partial y_D} = \frac{(\theta_3+2)}{2} E_3 y_D^{\frac{3-D_3+2\theta_3}{2}}\left[A_3 I_{\frac{1-D_3}{2+\theta_3}}\left(E_3 y_D^{\frac{2+\theta_3}{2}}\right) - B_3 K_{\frac{1-D_3}{2+\theta_3}}\left(E_3 y_D^{\frac{2+\theta_3}{2}}\right)\right]. \quad (31)$$

Applying the boundary condition, the coefficients can be solved. Based on the inner boundary condition $\bar{p}_{2fD}|_{y_D=d_D} = \bar{p}_{3fD}|_{y_D=d_D}$, we have

$$\bar{p}_{2fD}|_{y_D=d_D} = d_D^{\frac{3+\theta_3-D_3}{2}}\left[A_3 I_{\frac{3+\theta_3-D_3}{2+\theta_3}}\left(\frac{2w_3^{0.5}}{2+\theta_3} d_D^{\frac{2+\theta_3}{2}}\right) + B_3 K_{\frac{3+\theta_3-D_3}{2+\theta_3}}\left(\frac{2w_3^{0.5}}{2+\theta} d_D^{\frac{2+\theta_3}{2}}\right)\right] - \frac{v_3}{w_3}. \quad (32)$$

Considering the outer boundary condition $a_{34}\frac{\partial \bar{p}_{3fD}}{\partial y_D}|_{y_D=l_D} = (\frac{\partial \bar{p}_{4D}}{\partial y_D} - \frac{g_{4D}}{u})|_{y_D=l_D}$ and using the solution of Region 4, we can obtain

$$a_{34}\frac{\theta_3+2}{2} E_3 l_D^{\frac{3-D_3+2\theta_3}{2}}\left[A_3 I_{\frac{1-D_3}{2+\theta_3}}\left(E_3 l_D^{\frac{2+\theta_3}{2}}\right) - B_3 K_{\frac{1-D_3}{2+\theta_3}}\left(E_3 l_D^{\frac{2+\theta_3}{2}}\right)\right] = \left(F_{43}\bar{p}_{3fD}|_{y_D=l_D} - F_{43}d_4 - \frac{g_{4D}}{u}\right)\Big|_{y_D=l_D}. \quad (33)$$

Here, $\bar{p}_{3fD}|_{y_D=l_D}$ can be given by Eq. (34), namely,

$$\bar{p}_{3fD}|_{y_D=l_D} = l_D^{\frac{3+\theta_3-D_3}{2}}\left[A_3 I_{\frac{3+\theta_3-D_3}{2+\theta_3}}\left(\frac{2w_3^{0.5}}{2+\theta_3} l_D^{\frac{2+\theta_3}{2}}\right) + B_3 K_{\frac{3+\theta_3-D_3}{2+\theta_3}}\left(\frac{2w_3^{0.5}}{2+\theta_3} l_D^{\frac{2+\theta_3}{2}}\right)\right] - \frac{v_3}{w_3}. \quad (34)$$

Therefore, the derivative of pressure with respect to position can be expressed by

$$\left.\frac{\partial \bar{p}_{3fD}}{\partial y_D}\right|_{y_D=d_D} = F_{32}\bar{p}_{2fD}|_{y_D=d_D} + Z_3, \quad (35)$$

where F_{32} and Z_3 can be derived by A_3 and B_3 in Eq. (31).

(3) Solutions of Region 2

The dimensionless diffusion equations of Region 2 in the Laplace domain are given by

$$\begin{cases} (1-\omega_2)u\bar{p}_{2mD} + \lambda_2\left(\bar{p}_{2mD} - \bar{p}_{2fD} + \frac{p_{cD}}{u}\right) = 0, \\ \frac{\partial^2 \bar{p}_{2fD}}{\partial y_D^2} + \frac{D-\theta-2}{y_D}\frac{\partial \overline{p}_{2fD}}{\partial y_D} + \left(\frac{y_D}{w_{fD}/2}\right)^{\theta}\frac{(1-\omega_2)u\lambda_2}{(1-\omega_2)u+\lambda_2}\left(\frac{p_{cD}}{u}\right) + \left(\frac{y_D}{w_{fD}/2}\right)^{\theta}\frac{\mu_2 k_{mw}}{\mu_5 k_{fw}}\left(\frac{\partial \bar{p}_{5D}}{\partial x_D} - \frac{g_{5D}}{u}\right)\Big|_{x_D=x_{fD}} \\ \quad = \left(\frac{y_D}{w_{fD}/2}\right)^{\theta_f}\left(\omega_2 u + \frac{(1-\omega_2)u\lambda_2}{(1-\omega_2)u+\lambda_2}\right)\bar{p}_{2fD}, \\ \bar{p}_{2fD}|_{y_D=\frac{w_{fD}}{2}} = \bar{p}_{1D}|_{y_D=\frac{w_{fD}}{2}}, \\ \frac{k_{2f}}{\mu_2}\left.\frac{\partial \bar{p}_{2fD}}{\partial y_D}\right|_{y_D=d_D} = \frac{k_{3f}}{\mu_3}\left.\frac{\partial \bar{p}_{3fD}}{\partial y_D}\right|_{y_D=d_D}. \end{cases} \quad (36)$$

The dimensionless diffusion equations of the fracture system in Region 2 become

$$\frac{\partial^2 \overline{p}_{2fD0}}{\partial y_D^2} + \frac{D-\theta-2}{y_D}\frac{\partial \overline{p}_{2fD0}}{\partial y_D} + \left\{\begin{array}{l} \frac{(1-\omega_2)u\lambda_2}{(1-\omega_2)u+\lambda_2}\frac{p_{cD}}{u} \\ \quad -\frac{\mu_2 k_{mw}}{\mu_5 k_{fw}}\frac{g_{5D}}{u} + \left[\frac{k_{mw}}{k_{fw}}F_{52}\right. \\ \quad \left. -\left(\omega_2 u + \frac{(1-\omega_2)u\lambda_2}{(1-\omega_2)u+\lambda_2}\right)\right]\overline{p}_{2fD0} \end{array}\right\} \times \left(\frac{y_D}{w_{fD}/2}\right)^{\theta} = 0. \quad (37)$$

The general form of solution for Eq. (37) is given by

$$\overline{p}_{2fD0} = y_D^{\frac{3+\theta-D}{2}} \left[AI_{\frac{3+\theta-D}{2+\theta}} \left(\frac{2(C_1C_2)^{0.5}}{2+\theta} y_D^{\frac{2+\theta}{2}} \right) + BK_{\frac{3+\theta-D}{2+\theta}} \left(\frac{2(C_1C_2)^{0.5}}{2+\theta} y_D^{\frac{2+\theta}{2}} \right) \right] - C_3. \tag{38}$$

Using the inner and outer boundary conditions, the coefficients in Eq. (38) can be calculated. Substituting the coefficients of A and B into Eq. (37), we can obtain

$$\left. \frac{\partial \overline{p}_{2fD0}}{\partial y_D} \right|_{y_D=\frac{w_{fD}}{2}} = F_{21} \overline{p}_{1D0}|_{y_D=\frac{w_{fD}}{2}} + Z_2, \tag{39}$$

where F_{21} and Z_2 can be derived by A and B in Eq. (38).

(4) Solutions of Region 1

The dimensionless diffusion equations of the primary region in the Laplace domain are given by

$$\begin{cases} \dfrac{\partial^2 \overline{p}_{1D0}}{\partial x_D^2} + a_{21} \left. \dfrac{\partial \overline{p}_{2fD0}}{\partial y_D} \right|_{y_D=\frac{w_{fD}}{2}} - u\eta_{21} \overline{p}_{1D0} = 0, \\ \left. \dfrac{\partial \overline{p}_{1D0}}{\partial x_D} \right|_{x_D=0} = \dfrac{c}{u}, \quad \left. \dfrac{\partial \overline{p}_{1D0}}{\partial x_D} \right|_{x_D=1} = 0. \end{cases} \tag{40}$$

According to the results of Region 2, substituting Eq. (39) into Eq. (40), the solution of the bottom hole pressure in Laplace domain at the wellbore is

$$\bar{p}_{1D} = \frac{r_{12}\mathrm{e}^{r_{11}x_D} - r_{11}\mathrm{e}^{r_{11}-r_{12}}\mathrm{e}^{r_{12}x_D}}{ur_{11}r_{12}(1-\mathrm{e}^{r_{11}-r_{12}})} c + \frac{a_{21}Z_{21}}{u\eta_{21} - a_{21}F_{21}}. \tag{41}$$

To incorporate the impacts of the wellbore storage and skin factor into the dimensionless wellbore pressure, Duhamel's principle[31] is used as follows:

$$\bar{p}_{wD} = \frac{u\bar{p}_{1D}|_{xD=0} + S}{u[1 + uC_D(u\bar{p}_{1D}|_{xD=0} + S)]}. \tag{42}$$

The dimensionless of the bottom hole production rate in the Laplacian domain can be given by

$$\bar{q}_{wD}(u) = \frac{1}{u^2 \bar{p}_{wD}(u)}. \tag{43}$$

To acquire solutions in real-time space, the bottom hole production rate of a single fracture well in time domain can be obtained by the numerical Laplace inversion method.[32] Finally, the accumulative production rate can be calculated by

$$Q_D = \int_0^t q_{wD}(t)\mathrm{d}t. \tag{44}$$

3.2. Model Validation

We have developed a new seven-region analytical model for MFHW in the tight oil reservoir, which can thoroughly consider the effects of fractal, imbibition and non-Darcy flow on the production performance of tight oil reservoirs. To validate the new model, we compare our model results with one subject well from Cardium tight oil formation.[33] The subject well is an open hole with 10 stages, and it is the transverse hydraulic fracture. The basic wellbore and oil reservoir data for this well are listed in Table 2. We also set the parameter values of the new model to be consistent with the parameter values of the subject well. Besides, the matching parameters with those highlighted with the asterisk are also listed. The values of the matching parameters can be varied according to different oilfield characteristics, but they should meet the basic characteristics of low permeability reservoir obtained in field measurement. To show the effects of fractal, imbibition and non-Darcy flow on the production performance analysis, six different combinations of influencing factors (case 1: no imbibition and Darcy flow; case 2: imbibition and Darcy flow; case 3: no imbibition and non-Darcy flow; case 4: imbibition and non-Darcy flow; case 5: imbibition and fractal; case 6: imbibition, non-Darcy flow and fractal) are studied, which are shown in Fig. 3. The results of case 3 and case 4 indicate that the imbibition effect is an important factor in the fractured reservoir exploitation, which cannot be neglected. In case 2 and case 4, the production rate curve without considering non-Darcy flow can be obtained under the condition of considering imbibition. It demonstrates that the influence of non-Darcy flow is of great importance in the production performance analysis. The effects of imbibition, fractal and non-Darcy flow are all considered on the oil reservoir productivity in case 6. It can be seen that the model result of case 6 is in good agreement with the production rate of the subject well, which proved that the mathematical model and its algorithm are effective and reliable for predicting reservoir productivity in the actual oil field. Thus, the developed seven-region analytical model can be used to analyze the production performance of MFHW in the tight oil reservoir,

Table 2 Input Wellbore and Oil Reservoir Data.

Parameters	Value	Parameters	Value
Reservoir length, L_R, m	1320	*Porosity of Region 2 and 3, $\phi_{j(f+m)}$	0.16
Reservoir width, W, m	700	Fracture porosity, ϕ_f	0.2
Formation thickness, h, m	5	Fracture permeability, k_f, mD	10,000
Horizontal well length, LH, m	1178	Matrix porosity, ϕ_m	0.12
*HF half length, x_f, m	130	Matrix permeability, k_m, mD	0.28
HF width, w_f, m	0.003	Compressibility of matrix, C_{tm}, MPa^{-1}	0.0019
*Width of imbibition zone, d, m	20	*Skin factors, S	2
*Width of Region 2 and 3, l, m	60	Initial water saturation, Sw_i	0.14
Initial formation pressure, p_i, MPa	13.9	*Wetting angle, β, degree	45
Bottom pressure, p_w, MPa	1.8	*TPG, G, MPa/m	0.011
Oil viscosity, μ, MPa·s	1.414	Shape factor, α, m^{-2}	0.12
Oil volume factor, B	1.19	Fractal dimension, D	1.95
Fracture number, N_F	10	Fractal index, θ	0.01

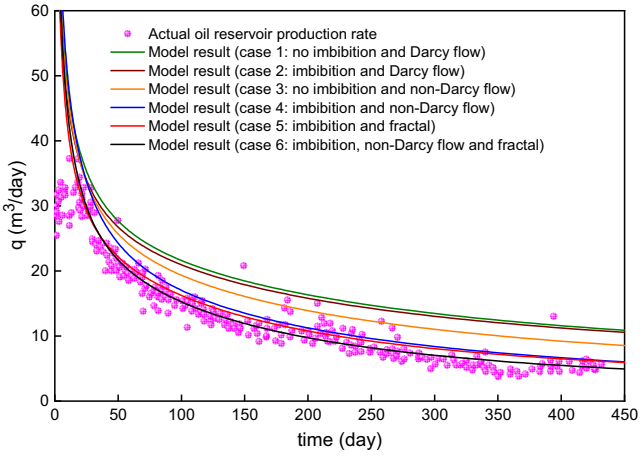

Fig. 3 Comparisons of production rate for the field examples.

and the effects of fractal, imbibition and non-Darcy flow should not be ignored in the production performance analysis.

3.3. Sensitivity Analysis on Deliverability Evaluation

In this section, the different influencing factors, including the fractal, imbibition and threshold pressure gradient on the productivity of horizontal wells, are quantitatively analyzed. The simulation parameters and their values are listed in Table 3.

3.3.1. *Influence of fractal on reservoir deliverability*

To describe the heterogeneity of fracture networks on oil reservoir production performance, the fractal theory[34–36] based on self-similarity and scale invariance of the fracture network is applied. In this work, the fractal dimension D and fractal index θ are employed to consider the effect of fractal on the oil reservoir productivity. In the new model, Region 2 and Region 3 exist in fractal fracture networks. Both of them are deformable double media regions, where both fractures and matrix exist. D denotes the fractal dimension of both the fracture medium and matrix medium with $D_f = D_m = D$, θ stands for the fractal index of the fracture with $\theta_f = \theta$, and the fractal index of the matrix θ_m is set to 0, which means there is no abnormal conductivity in the rock medium fractals. The relationships between the permeability, porosity and the fractal dimension, fractal index of the fracture system and matrix system can be referred to in Eqs. (1) and (2). The dimensionless accumulative production rate Q_D is calculated based on Eq. (44). Figures 4 and 5 exhibit the accumulative production rate of different fractal oil reservoirs.

From Fig. 4a, we can see that the fractal dimension of Region 2 has a significant influence on the oil reservoir deliverability. The dimensionless accumulative production rates obviously increase in the initial stage due to the wellbore storage and skin effect. With the fractal dimension D_2 rising from 1.9 to 2.1, the dimensionless accumulative production rate significantly grows from 5.8 to 13.8, which is increased by almost 1.4 times. The value of fractal dimension equaling 2 means the traditional Euclidean dual-porosity model, i.e. no fractal characteristics in the SRV. When the value of fractal dimension is not 2, the proposed model is converted to non-homogenous reservoir modeling, which indicates the geometric property of the natural-fracture and induced-fracture network, and the heterogeneity becomes more complex

Table 3 Input Model Parameters and their Values.

Parameters	Value	Parameters	Value
Reservoir length, L_R, m	1200	Cluster number, nc	2
Reservoir width, W, m	600	Fracture porosity, ϕ_f	0.0045
Formation thickness, h, m	10	Fracture permeability, k_f, mD	20,000
Horizontal well length, LH, m	1140	Matrix porosity, ϕ_m	0.12
HF half-length, x_f, m	150	Matrix permeability, k_m, mD	0.1
HF width, w_f, m	20	Compressibility of matrix,C_{tm}	0.0005
Width of imbibition zone, d, m	20	Shape factor, α, m^{-2}	0.12
Width of Region 2 and 3, l, m	60	Initial water saturation, Sw_i	0.2
Initial formation pressure, p_i, MPa	15	Wetting angle, β, degree	45
Bottom pressure, p_b, MPa	10	TPG, G, MPa/m	0.01
Oil viscosity, μ, MPa·s	5	*Skin factors, S	0.12
Oil volume factor, B	1.01	Fractal dimension, D	1.95
Fracture number, N_F	15	Fractal index, θ	0
Wellbore storage coefficient, C_{Dxf}	10,000		

and stronger. However, with the increase of fractal index of Region 2, the dimensionless accumulative production rate decreases obviously because the natural-fracture and induced-fracture networks in the SRV region provide the main liquid yield of MFHW at this time. In general, the larger the fractal dimension and the smaller the fractal index in Region 2, the higher the oil reservoir deliverability obtained.

Figure 5 illustrates the impacts of fractal dimension and fractal index of Region 3 on the production performance of the MFHW. Results indicate that the increment of fractal dimension in Region 3 cannot improve the dimensionless accumulative production rate significantly, which is very different from that in Region 2. While the trend of dimensionless accumulative production rate with fractal index in Region 3 is similar to that in Region 2. With the rise of the fractal index of Region 3, the dimensionless accumulative production rate reduces gradually. The fractal index indicates the migration distance of fluid in the fracture network. The smaller the fractal index is, the shorter the migration path of fluid is. That's why the smaller fractal index will be beneficial to fluid diffusion and reservoir deliverability.

From Figs. 4 and 5, it can be observed that the choice of the fractal dimension has a significant impact on the solutions throughout the production period. With the increase of fractal dimension and the decrease of fracture porosity and matrix-fracture channel flow along the fracture, the production increases gradually. The permeability attenuation also increases as the fractal index becomes large, resulting in the decrease of early production. This result indicates that the fracturing support system should be optimized during fracturing operation to ensure the flow capacity of the support fracture network and improve production.

3.3.2. *Influence of imbibition on reservoir deliverability*

Next, the effect of imbibition on the reservoir deliverability is specifically analyzed. The imbibition effect occurs in Region 2, where the fracturing fluid sweeps into this region resulting in both imbibition and cross-flow. The capillary pressurep_c depends on the wettability angle β, the relationship between them can be referred to in Eq. (3). In general, different oil reservoirs have different wettability of rock, and different wettability can affect the imbibition behavior. In this study, the wettability angle of the formation rock is changed to different values, both the daily and accumulative production rates are calculated. Besides, the contributions of imbibition on the daily and accumulative production rates are defined as: $\Delta q = q_{\text{with imbibition}} - q_{\text{no inmbibition}}$ and $\Delta Q = Q_{\text{with imbibition}} - Q_{\text{no imbibition}}$, respectively. Here, $q_{\text{no inmbibition}}$ and $Q_{\text{no imbibition}}$ denote the daily and accumulative production rates at $\beta = 90°$.

Figures 6a and 6b show the influences of wettability angle on the dimensionless daily and accumulative production rates. It can be seen that the wetting angle β has an important impact on the reservoir production. In terms of the daily production rate, the smaller the wetting angle β is, the stronger the imbibition effect will be. When $\beta \leq 90°$ (water wettability), the stronger the imbibition effect is, the greater the daily production rate

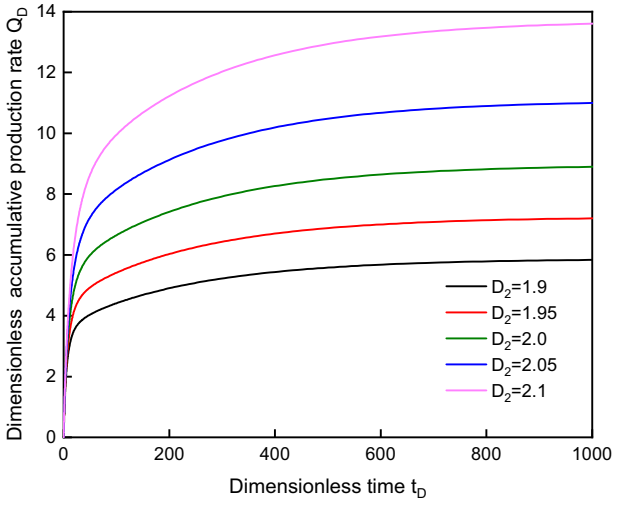

(a)

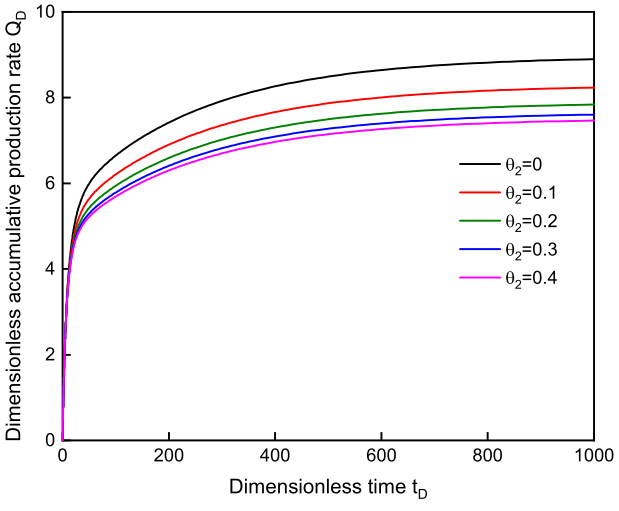

(b)

Fig. 4 The influence of fractal structure of Region 2 on the reservoir deliverability (only considering the fractal effect in Region 2, and Region 3 is a traditional reservoir with $D_3 = 2$ and $\theta_3 = 0$): **(a)** Effect of fractal dimension D_2 on dimensionless accumulative production rate ($\theta_2 = 0$); **(b)** Effect of fractal index θ_2 on dimensionless accumulative production ($D_2 = 1.95$).

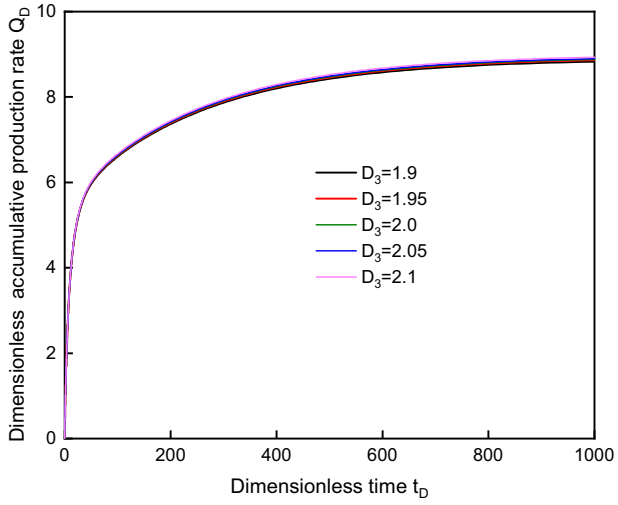

(a)

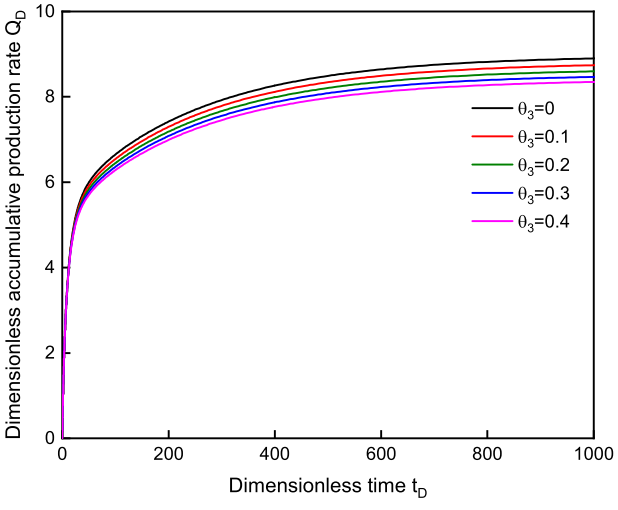

(b)

Fig. 5 The influence of fractal structure of Region 3 on the reservoir deliverability (only considering the fractal effect in Region 3, and Region 2 is a traditional reservoir with $D_2 = 2$ and $\theta_2 = 0$): **(a)** Effect of fractal dimension D_3 on dimensionless accumulative production rate ($\theta_3 = 0$); **(b)** Effect of fractal index θ_3 on dimensionless accumulative production ($D_3 = 1.95$).

will be. When $\beta > 90°$ (oil wettability), the imbibition is not conducive to improving the daily production rate. The law of the accumulative yield is consistent with the daily reservoir production. As the wetting angle increases from 0° to 150°, the dimensionless accumulative production rate obviously cuts down from 9.4 to 7.1 throughout the production period, which is decreased by almost 25% of the maximum production. From Fig. 6c, we can find that the accumulative production rate induced by imbibition becomes positive when the wettability is water-wet, and the imbibition is caused by water being imbibed into the matrix and oil being discharged into the fractures. When the reservoir rock is oil-wet, the accumulative production rate caused by imbibition effect turns negative, which means that the imbibition is not beneficial to reservoir production. This is because the effect of imbibition is reduced in this case, and oil flows from the matrix into the fracture for differential pressure, resulting in lower daily and cumulative production rates. Thus, the stronger the impact of imbibition

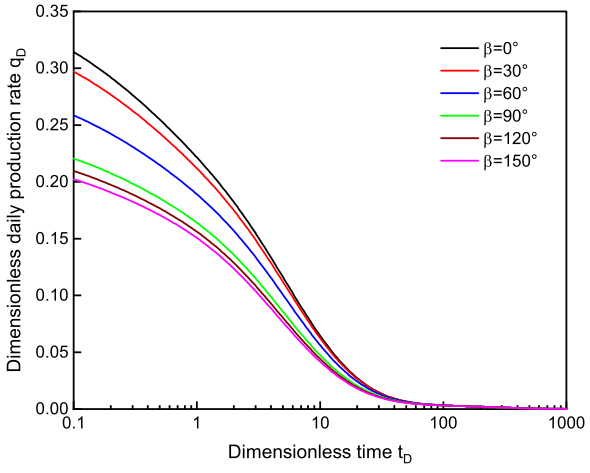

(a)

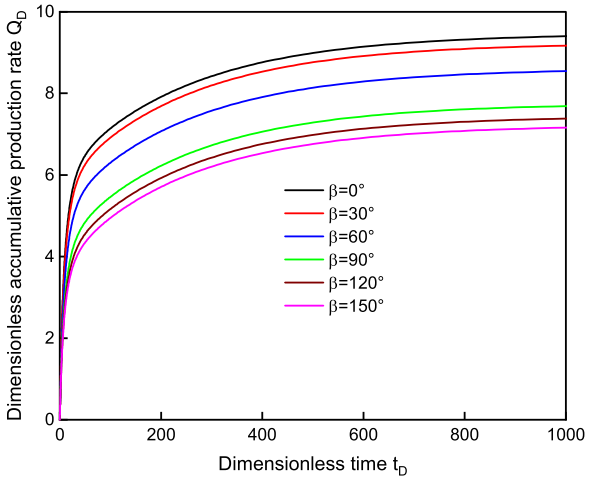

(b)

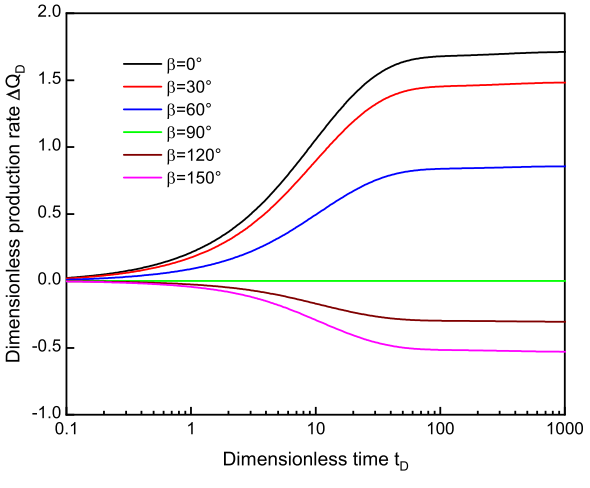

(c)

Fig. 6 The influence of imbibition on the reservoir deliverability: **(a)** Effect of wetting angle β on dimensionless daily production rate; **(b)** Effect of wetting angle β on dimensionless accumulative production rate; **(c)** Contributions of imbibition on accumulative production rate.

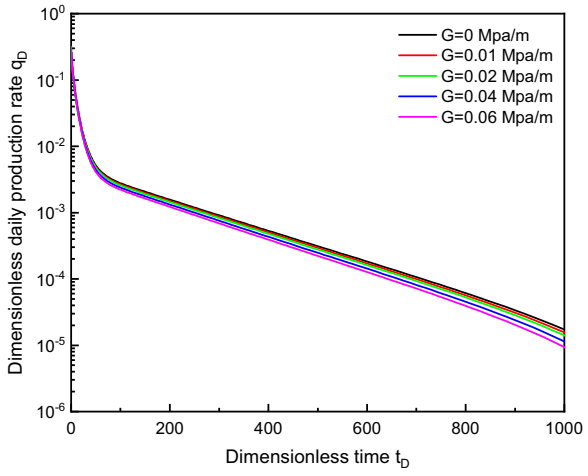

(a)

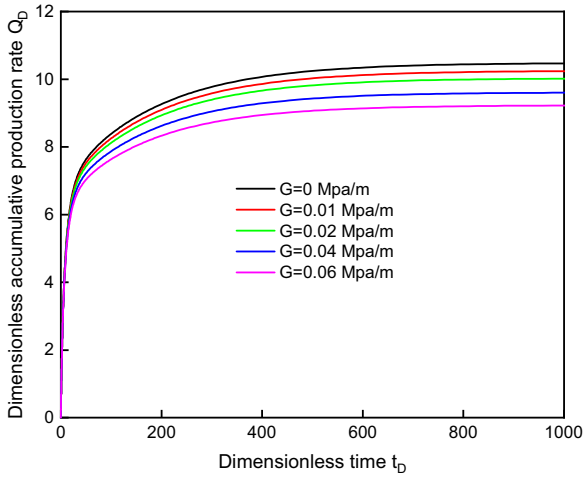

(b)

Fig. 7 The influence of TPG on the reservoir deliverability: **(a)** Effect of TPG on dimensionless daily production rate; **(b)** Effect of TPG on dimensionless accumulative production rate.

is, the more oil can be produced in the formation, and simultaneously the earlier daily production and later accumulative production will increase.

3.3.3. *Influence of threshold pressure gradient on reservoir deliverability*

Non-Darcy flow exists in tight oil reservoirs due to the presence of nanopores. The effect of threshold pressure gradient on the oil reservoir deliverability is unable to be ignored when describing the fluid flow in a porous medium for production performance. In this work, the effect of non-Darcy flow in Regions 4, 5, 6 and 7 on the daily and accumulative

production rates are quantitatively discussed. As shown in Fig. 7a, it can be seen that the influence of threshold pressure gradient on the daily productivity is not so much obvious. However, there exists an obvious variation of dimensionless accumulative production rate as the change of threshold pressure gradient. With the threshold pressure gradient rising from 0 MPa/m to 0.06 MPa/m, the dimensionless accumulative production rate gradually decreases from 10.5 to 9.2 in the entire production period, which is reduced by nearly 12% of the productivity without considering threshold pressure gradient effect. It can be seen that there is a negative correlation between the threshold pressure gradient and the oil reservoir production. This is because the higher the threshold pressure gradient, the greater the resistance of the fluid to flow through the formation.

4. CONCLUSION

In this paper, to obtain a more detailed description of the production of multi-stage fractured horizontal wells, a seven-region semi-analytical mathematical model considering the influences of the fractal, imbibition and non-Darcy flow in the fractal reservoir is newly developed and solved at length. A field example is conducted to verify the validity of the mathematical model. Based on the model, the effects of the fractal, imbibition and non-Darcy flow on the deliverability of MFHW in tight oil reservoir are concretely investigated. The simulation results lead to the following conclusions:

(1) Unlike the conventional fracture model with uniform distribution of fracture proppant, the present proposed model can better explain the heterogeneity of fracture network within dual-porosity SRV and dual-porosity. The solution of seven-region semi-analytical model can provide a suitable algorithm for the deliverability evaluation in tight oil reservoirs.
(2) The fractal plays a predominant influence on the productivity of MFHW in tight oil reservoirs. The larger the fractal dimension and the smaller the fractal index is, the higher the accumulative production rate can finally be obtained. The fractal effect of fracture network must be considered in the oil reservoir production performance analysis.
(3) The imbibition has important effect on the deliverability of MFHW in tight oil reservoirs. As the increasing of wetting angle, the daily and accumulative production rates obviously reduce. In the water-wet formations, the imbibition has a positive impact on the production rate, while it has a negative impact on the production rate in the oil-wet formations.
(4) Compared with the fractal and imbibition, the threshold pressure gradient has less influence on the production of MFHW in tight oil reservoirs. The result suggests that there is a negative correlation between the threshold pressure gradient and production performance. The small threshold pressure gradient will be beneficial to the accumulative production rate.

ACKNOWLEDGMENTS

Supports given by the National Natural Science Foundation of China (Grant Nos. 11872062 and 12102419) and the China Scholarship Council (Grant No. 2020083301145) are gratefully acknowledged.

ORCID

W. Yan https://orcid.org/0000-0002-8640-6700

REFERENCES

1. Y. W. He, S. Q. Cheng, J. Z. Qin, Z. Chai, Y. Wang, S. Patil, M. Li and H. Y. Yu, Analytical interference testing analysis of multi-segment horizontal well, *J. Pet. Sci. Eng.* **171** (2018) 919–927.
2. A. Wasaki and I. Y. Akkutlu, Permeability of organic-rich shale, *SPE J.* **5** (2015) 1384–1396.
3. B. Yan, Y. Wang and J. E. Killough, Beyond dual-porosity modeling for the simulation of complex flow mechanisms in shale reservoirs, *Comput. Geosci.* **20** (2016) 69–91.
4. B. Q. Xiao, H. Z. Zhu, F. Y. Chen, G. B. Long and Y. Li, A fractal analytical model for Kozeny–Carman constant and permeability of roughened porous media composed of particles and converging-diverging capillaries, *Powder Technol.* **420** (2023) 118256.
5. S. S. Yao, F. H. Zeng, H. Liu and G. Zhao, A semi-analytical model for multi-stage fractured horizontal wells, *J. Hydrol.* **507** (2013) 201–212.
6. C. L. Cipolla, N. R. Warpinski and M. J. Mayerhofer, Hydraulic fracture complexity: Diagnosis, remediation, and explotation, in *Paper SPE 115771 Presented at the SPE Asia Pacific Oil and Gas Conference and Exhibition*, Perth, Australia, 20–22 October 2008.

7. M. J. J. Mayerhofer, E. P. P. Lolon, N. R. R. Warpinski, C. L . L. Cipolla, D. Walser and C. M. M. Rightmire, What is stimulated reservoir volume? *SPE Prod. Oper.* **25** (2010) 89–98.
8. X. W. Weng, Modeling of complex hydraulic fractures in naturally fractured formation, *J. Unconv. Oil Gas Resour.* **9** (2015) 114–135.
9. M. E. Brown, E. Ozkan, R. Raghavan and H. Kazemi, Practical solutions for pressure-transient responses of fractured horizontal wells in unconventional shale reservoirs, *SPE Reserv. Eval. Eng.* **14** (2011) 663–676.
10. E. Stalgorova and L. Mattar, Practical analytical model to simulate production of horizontal wells with branch fractures, in *Paper SPE 162515 Presented at SPE Canadian Unconventional Resources Conference*, Calgary, Alberta, 30 October 2012.
11. E. Stalgorova and L. Mattar, Analytical model for unconventional multifractured composite systems, *SPE Reserv. Eval. Eng.* **16** (2013) 246–256.
12. J. H. Ji, Y. D. Yao, S. Huang, X. Q. Ma, S. Zhang and F. Z. Zhang, Analytical model for production performance analysis of multi-fractured horizontal well in tight oil reservoirs, *J. Pet. Sci. Eng.* **158** (2017) 380–397.
13. B. Yuan, Y. L. Su, R. G. Moghanloo, Z. H. Rui, W. W. Wang and Y. Y. Shang, A new analytical multi-linear solution for gas flow toward fractured horizontal wells with different fracture intensity, *J. Nat. Gas Sci. Eng.* **23** (2015) 227–238.
14. B. Q. Xiao, W. Wang, X. Zhang, G. B. Long, J. T. Fan, H. X. Chen and L. Deng, A novel fractal solution for permeability and Kozeny–Carman constant of fibrous porous media made up of solid particles and porous fibers, *Powder Technol.* **349** (2019) 92–98.
15. J. H. Qian, W. W. Yan, J. Zhou and P. Xu, Fractal analysis and numerical simulation on pulsating flow patterns in a three-dimensional bronchial tree, *Fractals* **29** (2021) 2150053.
16. A. J. Katz and A. H. Thompson, Fractal sandstone pores: implications for conductivity and pore formation, *Phys. Rev. Lett.* **54** (1985) 1325–1328.
17. J. C. Chang and Y. C. Yortsos, Pressure-transient analysis of fractal reservoirs, *SPE Form. Eval.* **5** (1990) 31–38.
18. J. A. Acuna and Y. C. Yortsos, Numerical construction and flow simulation in networks of fractures using fractal geometry, in *Paper SPE 22703 Presented at SPE Annual Technical Conference and Exhibition*, Dallas, Texas, 6–9 October 1991.
19. M. J. Cossio, G. J. J. Moridis and T. A. A. Blasingame, A semianalytic solution for flow in finite-conductivity vertical fractures by use of fractal theory, *SPE J.* **18** (2013) 83–96.
20. W. W. Wang, Y. L. Su, G. G. Sheng, M. J. Cossio and Y. Y. Shang, A mathematical model considering complex fractures and fractal flow for pressure transient analysis of fractured horizontal wells in unconventional reservoirs, *J. Nat. Gas Sci. Eng.* **23** (2015) 139–147.
21. M. C. Liang, C. G. Fu, B. Q. Xiao, L. Luo and Z. K. Wang, A fractal study for the effective electrolyte diffusion through charged porous media, *Int. J. Heat Mass Transf.* **137** (2019) 365–371.
22. M. C. Liang, Y. M. Liu, B. Q. Xiao, S. S. Yang, Z. K. Wang and H. M. Han, An analytical model for the transverse permeability of gas diffusion layer with electrical double layer effects in proton exchange membrane fuel cells, *Int. J. Hydrog. Energy* **43** (2018) 17880–17888.
23. F. Y. Wang, Z. C. Liu, J. Cai and J. Gao, A fractal model for low-velocity non-Darcy flow in tight oil reservoirs considering boundary-layer effect, *Fractals* **26** (2018) 1850077.
24. B. Q. Xiao, Q. W. Huang, H. X. Chen, X. B. Chen and G. B. Long, A fractal model for capillary flow through a single tortuous capillary with roughened surfaces in fibrous porous media, *Fractals* **29** (2021) 2150017.
25. N. W. Zhou, S. F. Lu, M. Wang, W. Liu, Y. Guan, H. K. Tan and Z. X. Wang, Applicability of fractal capillary pressure models to sandstones, *J. Pet. Sci. Eng.* **85** (2020) 106626.
26. P. D. Khurpade, L. K. Kshirsagar and S. Nandi, Characterization of heterogeneous petroleum reservoir of Indian sub-continent: An integrated approach of hydraulic flow unit-mercury intrusion capillary pressure-fractal model, *J. Pet. Sci. Eng.* **205** (2021) 108788.
27. J. A. Acuna, I. Ershaghi and Y. C. Yortsos, Practical application of fractal pressure-transient analysis in naturally fractured reservoirs, *SPE Form. Eval.* **10** (1995) 173–179.
28. J. C. Cai, E. Perfect, C. L. Cheng and X. Y. Hu, Generalized modeling of spontaneous imbibition based on Hagen–Poiseuille flow in tortuous capillaries with variably shaped apertures, *Langmuir* **30** (2014) 5142–5151.
29. P. L. Wang, B. Q. Xiao, J. Gao, H. Z. Zhu, M. X. Liu, G. B. Long and P. C. Li, A novel fractal model for spontaneous imbibition in damaged tree-like branching networks, *Fractals* **31** (2023) 2350010.
30. A. Prada and F. Civan, Modification of Darcy's law for the threshold pressure gradient, *J. Pet. Sci. Eng.* **22** (1999) 237–240.

31. A. Everdingen and W. Hurst, The application of the Laplace transformation to flow problems in reservoirs, *J. Pet. Technol.* **1** (1949) 305–324.
32. H. Stehfest, Algorithm 368: Numerical inversion of Laplace transforms, *Commun. ACM* **13** (1970) 47–49.
33. C. R. Clarkson and P. K. Pedersen, Production analysis of western Canadian unconventional light oil plays, in *Paper SPE 149005 Presented at SPE Resources Conference*, Calgary, Alberta, Canada, 15–17 November 2011.
34. B. Q. Xiao, Y. P. Li, G. B. Long and B. M. Yu, Fractal permeability model for power-law fluids in fractured porous media with rough surfaces, *Fractals* **30** (2022) 2250115.
35. J. Gao, B. Q. Xiao, B. L. Tu, F. Y. Chen and Y. H. Liu, A fractal model for gas diffusion in dry and wet fibrous media with tortuous converging-diverging capillary bundle, *Fractals* **30** (2022) 2250176.
36. B. Q. Xiao, J. Fang, G. B. Long, Y. Z. Tao and Z. J. Huang, Analysis of thermal conductivity of damaged tree-like bifurcation network with fractal roughened surfaces, *Fractals* **30** (2022) 2250104.